Fluorescence Imaging for Monitoring the Colocalization of Two Single Molecules in Living Cells

Ikuko Koyama-Honda, Ken Ritchie, Takahiro Fujiwara, Ryota Iino, Hideji Murakoshi, Rinshi S. Kasai, and Akihiro Kusumi

Kusumi Membrane Organizer Project, Exploratory Research for Advanced Technology Organization (ERATO/SORST), Japan Science and Technology Agency, Department of Biological Science, and The Institute for Advanced Research, Nagoya University, Nagoya, 464-8602, Japan

ABSTRACT The interaction, binding, and colocalization of two or more molecules in living cells are essential aspects of many biological molecular processes, and single-molecule technologies for investigating these processes in live cells, if successfully developed, would become very powerful tools. Here, we developed *simultaneous*, dual-color, single fluorescent molecule colocalization imaging, to quantitatively detect the colocalization of two species of individual molecules. We first established a method for spatially correcting the two full images synchronously obtained in two different colors, and then for overlaying them with an accuracy of 13 nm. By further assessing the precision of the position determination, and the signal/noise and signal/background ratios, we found that two single molecules in dual color can be colocalized to within 64–100 nm (68–90% detectability) in the membrane of cells for GFP and Alexa633. The detectability of true colocalization at the molecular level and the erroneous inclusion of incidental approaches of two molecules as colocalization have to be compromised at different levels in each experiment, depending on its purpose. This technique was successfully demonstrated in living cells in culture, monitoring colocalization of single molecules of E-cadherin fused with GFP diffusing in the plasma membrane with single molecules of Alexa633 conjugated to anti-E-cadherin Fab externally added to the culture medium. This work established a benchmark for monitoring the colocalization of two single molecules, which can be applied to wide ranges of studies for molecular interactions, both at the levels of single molecules and collections of molecules.

INTRODUCTION

Single-molecule imaging techniques are becoming very important tools for biophysical studies (Fujiwara et al., 2002; Iino et al., 2001; Schütz et al., 2000; Sheetz et al., 1989; Tardin et al., 2003). They have given researchers the ability to directly observe the motion and localization of individual single molecules in live cells. In particular, for signal transduction studies, they facilitate observations of the diffusion of individual receptor molecules in the plasma membrane (Lommerse et al., 2004; Sako et al., 2000; Suzuki et al., 2004, 2003) as well as the recruitment of each individual cytoplasmic signaling molecule to the plasma membrane (Lommerse et al., 2004; Mashanov et al., 2004; Murakoshi et al., 2004). However, for the single-molecule techniques to be truly useful for studies of the molecular processes in living cells, particularly the signal transfer processes in the plasma membrane, these technologies must be developed to allow direct observations of two molecules that are undergoing (transient) binding to each other and/or colocalization/correlated motion in the plasma membrane of living cells, because such interactions are the essence of many molecular functions.

Signal transduction in the plasma membrane often proceeds through the correlated actions of many signaling molecules. Classically, the interaction/binding of two molecular species was implied by the colocalization of the two molecular species, as observed through bulk, multicolor fluorescence microscopy (or by biochemical and molecular biological techniques, such as immuno-coprecipitation, pull-down assays, and two-hybrid results). However, conventional fluorescence microscopy can only visualize the assembly of two molecular species when many molecules of each species are recruited, whereas most signaling events involve only one or two molecules of a single species. Furthermore, even when many molecules of a single species may be involved, if the residency time of each recruited molecule is short, which may be common in many signaling pathways, then the detectability of molecular interactions will fall rapidly. Therefore, advanced technologies that allow us to observe dynamic processes, like the transient assembly of only a few signaling molecules, are required. With this goal in mind, we have developed a method to directly and simultaneously image two individual signaling molecules (each labeled with a different color) in living cells through simultaneous, dual-color, single-molecule fluorescence microscopy. In fact, such single-molecule methods, including the single-molecule fluorescence resonance energy transfer (FRET) technique recently developed by Murakoshi et al. (2004), might be the only ways to directly visualize the signal transfer process, by examining the recruitment of

Submitted July 4, 2004, and accepted for publication October 14, 2004.

Address reprint requests to Dr. Akihiro Kusumi, Dept. of Biological Science, Nagoya University Chikusa-ku, Nagoya 464-8602, Japan. Tel.: 011-81-52-789-2969; Fax: 011-81-52-789-2968; E-mail: akusumi@bio.nagoya-u.ac.jp.

0006-3495/05/03/2126/11 $2.00

doi: 10.1529/biophysj.104.048967

upstream and downstream molecules, and the possible involvement of scaffolding proteins in that process.

Instrumentally, in our laboratory, the specimen was illuminated with two individual laser beams, using objective-lens-type total internal reflection fluorescence (TIRF), and the emission signals from the sample were chromatically separated by a dichroic mirror and filtered into two detection arms terminating in high-sensitivity cameras. However, the real issue here is that, to study live cells at the molecular level, tracking colocalization and/or correlated motion requires extremely high levels of spatial precision in the superposition of the two split images obtained at video rate or faster, and until this is done, the usefulness of single molecule technologies may be limited.

Colocalization at the level of single or small groups of molecules has been explored by several other groups. Kinosita et al. (1991) proposed the capture of two images shifted laterally depending either on their polarization or emission wavelength onto a single camera, before the single-molecule era. This technique was applied to imaging the orientation along actin filaments (using polarization) and calcium influxes into a cell (using fluorescence). No description was given regarding the accuracy of the method. For the practical purpose of performing single-molecule, two-color, simultaneous observations, it is much easier to have two separate gain controls over each of two cameras, rather than trying to use a single camera. Trabesinger et al. (2001) evaluated the statistical coincidental overlap events in vitro, thus putting the determination of the probability of overlap from a single image on firm statistical grounds, but did not propose a method for correcting for inherent aberrations in the dual-color imaging technique. Schütz et al. (1998) proposed a method to take two-color images on a single camera by rapidly alternating two excitation laser light sources (every 5 ms), and thus eliminated most of the distortions, except for chromatic aberrations, to obtain 40-nm accuracy for two colocalized single molecules in two colors. Morrison et al. (2003) and Karakikes et al. (2003) developed a spatial correction method for images of fixed cells taken sequentially on a single camera. Their spatial correction technique relies on determining the optical center of the image and calculating the radial shift of the images from that center through a single parameter, but the accuracy was limited to $\approx$300 nm. Lacoste et al. (2000) achieved an impressive 10-nm accuracy using bright fluorescent particles or quantum dots that can be excited with a single laser light and emit at separable wavelengths and through scanning the sample across a focused excitation laser. Though high in accuracy, this technique requires long times for image acquisition and, as described, is not applicable to imaging the motion of molecules in living cells.

In this research, we used a microscope with two detection arms equipped with high-sensitivity cameras working synchronously (at video rate or faster), to detect fluorescence signals chromatically separated by a dichroic mirror and filter sets. To achieve high precision in the colocalization of the two differently colored molecules in the two split images, the large systematic errors due to optical aberrations (like chromatic aberrations of the objective lens, and chromatic and other aberrations of the optics in the separate imaging paths) and camera-based effects must be corrected. We developed a method for spatially correcting the full video frame (covering all of the pixels in each frame) obtained on each arm, by first imaging a precise array of optical holes spanning the entire image in both observation paths (with optics used for the GFP-Alexa633 pair) using ''white-light'' bright-field transmission microscopy, and then performing a third-order spline fit across these arrays. Once the correction look-up table is made, the correction transformation is fast (12 s for 100 frames of 640 $\times$ 480 pixels or $\sim$1/4 of the video rate, using a 2.8-GHz Intel-PC machine) and was usually used to correct the entire sequence of the full frame images. A practical method to detect the colocalization of single molecules is proposed, based on the accuracies in the overlay and the determination of each molecule's position. This method is also applicable to single-molecule FRET imaging data (Murakoshi et al., 2004) and to split images projected on a single camera (Kinosita et al., 1991).

METHODS

Microscope setup

To simultaneously observe two single molecules (each labeled with a different color) in living cells, or more specifically, to view a molecule labeled by an organic dye (such as Alexa633) in the external leaflet of the membrane simultaneously with a green fluorescent protein (GFP)-tagged cytoplasmic protein, the homebuilt, objective-lens-type TIRF microscope, described previously (Iino et al., 2001) was modified. Fig. 1 shows a schematic diagram of the TIRF microscope we built to perform dual-color imaging at the level of single molecules. As the base, we used an Olympus IX-70 microscope with a modified mirror turret to allow the side entry of the excitation laser beams into the microscope. Excitation was performed through two laser beams steered into the microscope by a dual-color dichroic mirror (Chroma Technology, Rockingham, VT), to focus the beams at the back focal plane of the objective. We used an Olympus PlanApo 100$\times$ oil immersion objective with a numerical aperture of 1.4. For total internal reflection illumination, the incident laser beams were placed off the optical axis (but parallel to it) so that they would pass near the edge of the objective lens. Emission from the fluorophore was collected by the objective, past the dual-color excitation path dichroic, and was split into the two imaging systems by an observation path dichroic mirror. The image in each arm was projected on the photocathode of an image intensifier with a two-stage microchannel plate (C8600-03; Hamamatsu Photonics, Hamamatsu, Japan), which was lens-coupled to the camera. The cameras used were Hamamatsu electron bombardment charge-coupled device (EBCCD; C7190-23) or silicon intensified target (C2400-08) cameras. The cameras on the two detecting arms (side and bottom; two cameras of the same model number produced in the same batch were placed on each arm) were synchronized frame by frame by coupling the sync out of one camera to the trigger of the second (gen-locked). The camera images were stored on a digital video tape (PDV-184ME; Sony, Tokyo, Japan) for postexperiment spatial synchronization.

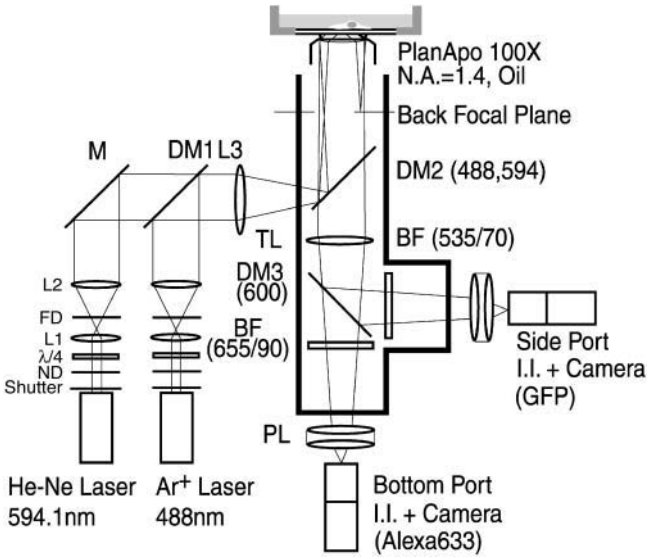

FIGURE 1 The microscope setup for simultaneous, dual-color, fluorescence imaging of two single molecules of different species. The optics and lasers indicated in this figure are those for the simultaneous observation of the pair of GFP and Alexa633. For the observations of other dyes, this microscope is equipped with the second harmonic Nd-YAG (532 nm) and He-Cd (442 nm) lasers and other appropriate optical components. The excitation arm consists of the following optical components: S, electronic shutter; ND, neutral density filter; $\lambda/4$, quarter-wave plate; L1 and L2, working as a 10× beam expander (L1, $f = 150$ mm; L2, $f = 15$ mm) for 488-nm excitation, or 4× beam expander (L1, $f = 80$ nm; L2, $f = 20$ mm) for 594-nm excitation; FD, field diaphragm; M, mirror, DM, dichroic mirror; L3, focusing lens ($f = 35$ mm); BP, band-pass filter. The two-color fluorescence emission signal is split by a dichroic mirror (*DM3*) and detected by two cameras at the side and bottom ports. TL, tube lens (1× or 2×); BF, barrier filter; PL, projection lens (2×); I.I, image intensifier.

Spatial corrections

To determine the individual characteristics of each imaging path, a predefined mask was simultaneously imaged through each path. This mask has a lattice of 1-μm diameter optical holes spaced 5-μm apart, as shown in Fig. 2. To produce this array of optical holes, a quartz slide glass was coated with a layer of chromium followed by a layer of chromium oxide, and then through photolithography, an array of 1-μm-diameter holes spaced 5 μm apart was produced (special order from Shibuya Kogaku, Wako, Japan). This grid allowed us to map a point, as imaged through one of the imaging paths, with the same point as imaged through the other path. The spatial accuracy of the center of the spot was 0.3 μm according to the manufacturer, and we assumed that optical holes were accurately spaced every 5 μm. This way, a (third-order) spline fit can be used to accurately correct for translations and rotations between the two observation arms, and for the optical distortions and inhomogeneities inherent in both the optical paths and each camera.

The algorithm for correcting the image obtained on each camera is as follows (shown in Fig. 3).

1. Set the two cameras (one at the side port and the other at the bottom port of the microscope) to obtain images of the mask, so that all of the holes from the mask on the images can be identified (i.e., by using a corner of the mask where the array of holes stops).
2. Capture a video sequence of 100 frames of the mask under bright-field illumination along both imaging paths. The contrast of the images should be as high as possible (a single-frame image is shown in Fig. 3 *A*).

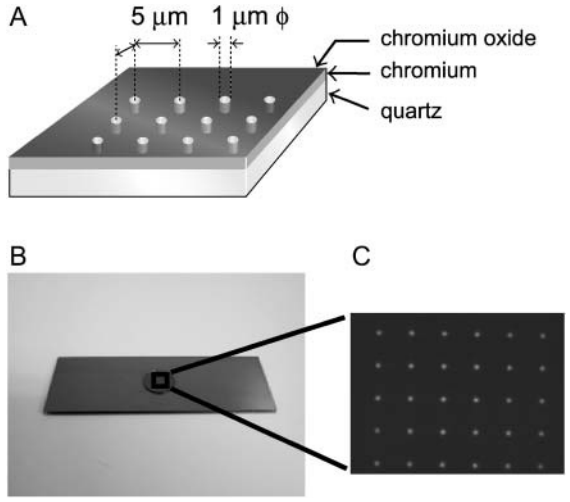

FIGURE 2 The mask used to spatially correct the dual-color images. (*A*) Schematic drawing, (*B*) the image, and (*C*) the magnified image of the mask. Layers of chromium and chromium oxide were deposited on a quartz slide glass. Photolithography was employed to make an array of holes.

3. Make an average image over the 100 video frames, obtained as above.
4. Make the average image binary by setting the threshold intensity such that spurious noise outside the array is minimized (Fig. 3 *B*).
5. For each dot, find the centroid.
6. Transform the images (see the next section) so that the dots are 5 μm apart (the manufacturer's specification for the accuracy of the center of the spot is 0.3 μm). Here we assume that this value of 5 μm is correct, and we correct both of the obtained images (on the side and the bottom ports) for this separation (the corrected images therefore contain distortions due to the irregularity of the array of the optical holes, but because these corrected images are distorted in the same way, these distortions do not affect the overlaying accuracy). To find the transform

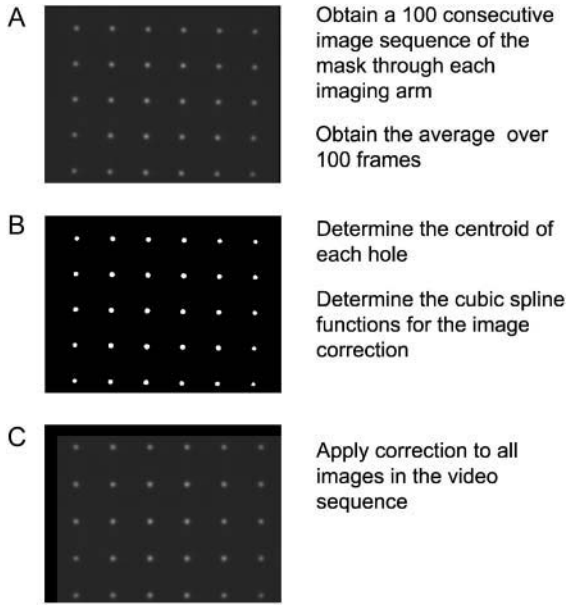

FIGURE 3 Algorithm for the spatial correction of the imaging arms of the microscope.

functions to carry out this operation, we fit the positions of the dots in the averaged image to third-order spline functions, which are then applied to the raw images to obtain the corrected images (see the next section and Appendix).

7. Apply the transform to the entire sequence of full-frame images from both cameras to obtain the corrected video image sequences (Fig. 3 *C*; see the next section).

Spatial transformation algorithm

The algorithm used to transform the uncorrected raw images to the spatially corrected images is as follows. For the centroids of the spots, a spline fit is applied along each row. The arc length between each pair of dots is set to 5 μm. This defines the corrected pixel locations along the horizontal axis for the image along these specific rows. From this, a spline fit is performed along the vertical axis at each of these corrected pixel positions, including the interpolated pixels in between the dots. This arc length between each pair of corrected pixel positions is again set to 5 μm. In this way, the corrected positions for the entire image are determined (see Appendix for more details).

Fluorescence intensity measurement

Alexa Fluor 633 carboxylic acid succinimidyl ester (Molecular Probes, Eugene, OR) conjugated to anti-CD59 Fab fragments (Alexa633-Fab; dye/protein = 0.3 by mol), and EGFP produced in *Escherichia coli* (BD Biosciences Clontech, Palo Alto, CA) were adsorbed on coverslips and covered with a layer of polyacrylamide gel (15%). They were simultaneously imaged at the level of single molecules by the two EBCCD cameras. Fluorescence images were digitized frame by frame, and the fluorescence signal intensities of 620 × 620 nm areas (8-bit images in 12 × 12 pixels) containing a single spot and the background intensities of the adjacent 620 × 620 nm areas were measured (Iino et al., 2001).

Analysis of the movement of single fluorescent molecules

The positions of these Alexa633-Fab and EGFP fluorescent spots fixed on coverslips were obtained and analyzed by a published method (Gelles et al., 1988; Kusumi et al., 1993; Sako et al., 1998). The positions (*x*- and *y*-coordinates) of each fluorescent spot were determined by software developed in our lab, based on the method of Gelles et al. (1988). The precision of the position determination for a single Alexa633-Fab or EGFP molecule was estimated using immobile Alexa633-Fab and EGFP molecules attached to the coverslip covered with 15% polyacrylamide gel.

Preparation of a standard sample for the determination of precision in two-color fluorescence imaging of single molecules in the cell

E-cadherin, a transmembrane protein responsible for the calcium-dependent cell-cell adhesion of epithelial tissues, was doubly labeled with GFP at its C-terminal cytoplasmic domain (Ecad-GFP) and with the Fab fragment of the anti-E-cadherin rat monoclonal antibody ECCD2 (Shirayoshi et al., 1986) conjugated with Alexa633 (Alexa-αEcad-Fab). This doubly labeled protein was observed as a standard sample for simultaneous, two-color, observations of single molecules. L cells, which do not express endogenous E-cadherin, were transfected with the cDNA for Ecad-GFP, and those stably expressing Ecad-GFP were cloned and maintained in Dulbecco's modified Eagle's medium with 10% fetal bovine serum (Iino et al., 2001). These cells were plated on 12 mm-ϕ coverslip-based dishes (Iwaki, Japan) and used two days later. The anti-E-cadherin antibody was digested with papain, and the anti-E-cadherin Fab fragments were purified by protein G column chromatography (Amersham, Buckinghamshire, UK) (Derrick and Wigley, 1994; Perosa et al., 1997). The anti-E-cadherin Fab fragments were conjugated with Alexa633, at an Alexa633/Fab molar ratio of ~0.7 (Alexa-αEcad-Fab). For the observation of fixed cells, the Ecad-GFP molecules expressed on the cell surface were labeled with the Alexa-αEcad-Fab by incubating the cells with 5.4 nM Alexa-αEcad-Fab for 15 min at room temperature. The cells were then fixed with 4% paraformaldehyde in Hanks' medium buffered with 2 mM PIPES (pH 7.4, called Hanks' buffer) for 1.5 h at room temperature. For live cell observations, L cells stably expressing Ecad-GFP molecules on the cell surface were incubated with 20 nM Alexa-αEcad-Fab for 2 min at 37°C and the microscope observation was carried out without washing away the unbound probe molecules. The Ecad-GFP molecule on the cell surface bound by an Alexa-αEcad-Fab molecule provides a convenient colocalization marker for testing our protocol for detecting colocalized molecules.

RESULTS AND DISCUSSION

Improvement of image superposition accuracies

All observations described here were carried out at video rate (30 frames/s). The results of the spatial correction are shown in Fig. 4 *A*. The top row shows the raw images of the mask taken by the two SIT cameras (the pixel size corresponds to 100 nm on the sample plane), whereas the bottom row shows the images after spatial correction. The accuracies of the overlay in the *x*- and *y*-directions were determined through the displacements in the measured positions of the same holes between the two averaged images (obtained on the side and bottom ports).

In the particular experiment using the SIT cameras, shown in Fig. 4 *A* (the mean deviations before the correction vary from experiment to experiment if the dichroic mirrors and cameras are reset, but the spread of the distribution remains about the same), the displacements between the raw images of the same hole ($12 \times 9 = 108$ holes) were spread over 320 and 230 nm (standard deviations 3.2 and 2.3 pixels with each pixel corresponding to 100 nm on the sample) for the *x*- and *y*-directions, respectively (Fig. 4 *B*, *left*). After the correction, the average *x*- and *y*-displacements over all holes were 0.9 ± 29 and -0.9 ± 20 nm for the *x*- and *y*-directions, respectively, as shown in Fig. 4 *B* (*right*). The standard deviations for the *x*- and *y*-displacements after the correction remained more or less comparable to these values, even if the dichroic mirrors and cameras were reset, and thus we defined the accuracy over the entire overlaid image (corrected images) as 29 and 20 nm (0.29 and 0.20 pixels) in the *x*- and *y*-directions, respectively.

The SIT camera has some level of retained image lag, so we often use an EBCCD camera for single fluorescent molecule observations. EBCCD cameras (or CCD cameras in general) have much less distortion as compared to SIT cameras, and the deviation of the displacement between two images of the same optically transparent hole without spatial correction was 66 and 42 nm (0.66 and 0.42 pixels) in the

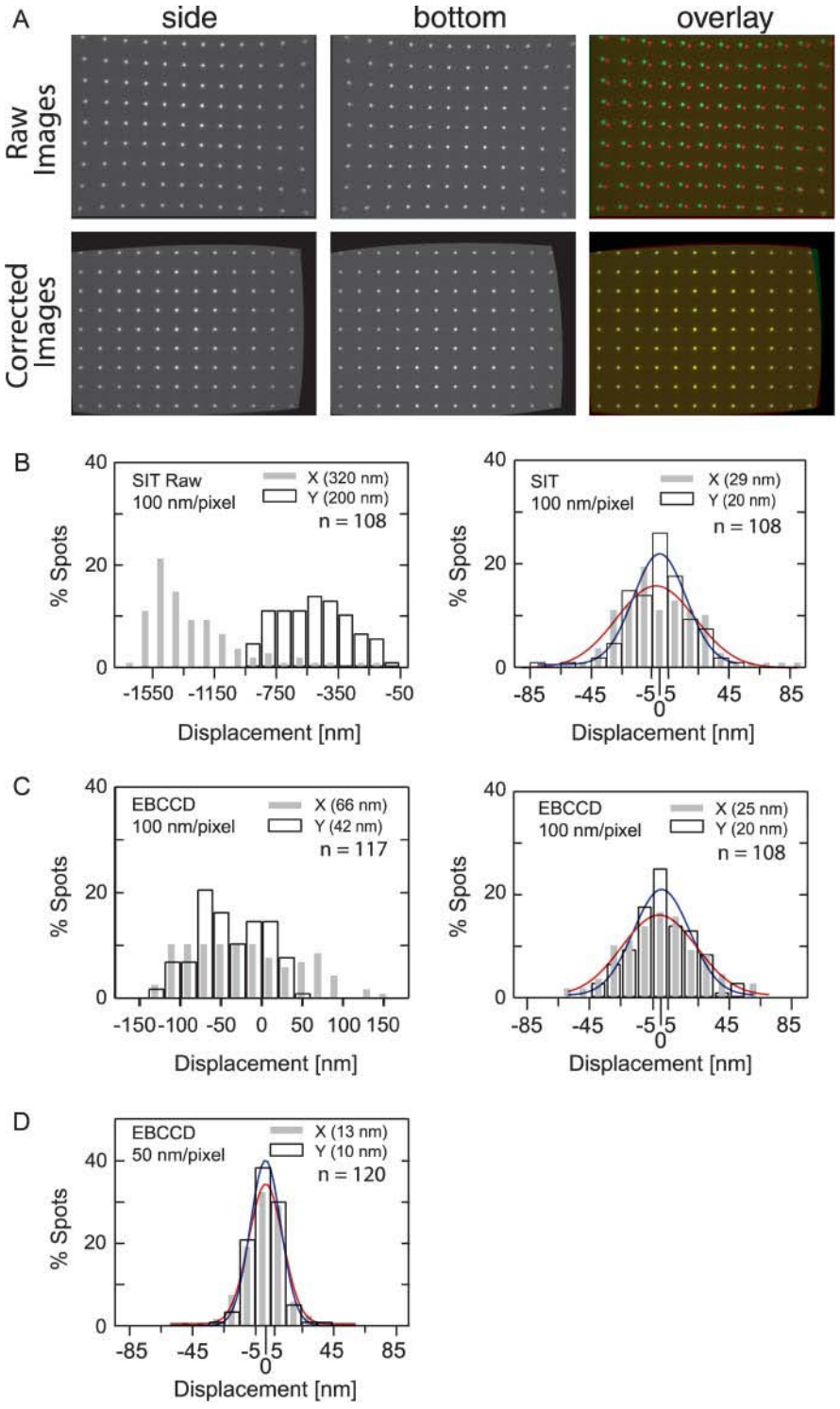

FIGURE 4 Improvement of superpositioning accuracy of simultaneously obtained, dual-color, single fluorescent molecule images by the spatial correction method developed here. (*A*, *top*) Images of the grid slide glass taken by two SIT cameras (100 nm on the sample/pixel) at the side (for GFP) and the bottom (for Alexa633) ports, and their overlaid images before correction. (*A*, *bottom*) Same series as the top after the spatial correction, as shown in Fig. 3. The ''white-light'' bright-field transmission microscopy was used with the same observation arms and optics used for simultaneous fluorescence observations, for the correction of chromatic aberrations. (*B*, *left*) Based on the raw images (*top* images in *A*), the histograms of the displacements in the *x*- and *y*-directions for all of the visible grid holes were obtained. The average displacements are -1300 ± 320 nm (*x*-direction, *shaded bar*) and -500 ± 230 nm (*y*-direction, *open bar*). The mean varies each time the dichroic mirrors or the cameras are reset, but the standard deviations (3.2 and 2.3 pixels in *x*- and *y*-directions, respectively) generally stay the same. (*B*, *right*) Based on the corrected images (*bottom* images in *A*), the histograms of the average displacements in the *x*- and *y*-directions for all of the visible grid holes were obtained. The average displacements are 0.9 ± 29 nm (*x*, *shaded bar*) and -0.9 ± 20 nm (*y*, *open bar*) (standard deviations 0.29 and 0.20 pixels in the *x*- and *y*-directions, respectively). The histograms were fitted by Gaussian curves (*x*, *red line*; *y*, *blue line*). (*C*) The same as panel *B*, but EBCCD cameras (100 nm on the sample/pixel) were used. (*Left*) The average displacements are -20 ± 66 nm and -39 ± 42 nm for the *x*- (*shaded*) and *y*- (*open*) directions, respectively, in this particular setting. Standard deviations are generally the same after resetting of the dichroic mirror and the camera, and are 0.66 and 0.42 pixels in the *x*- and *y*-directions, respectively. (*Right*) After the spatial correction. The average displacements are -1.1 ± 25 nm and 1.1 ± 20 nm in the *x*- and *y*-directions, respectively. Standard deviations were improved to 0.25 and 0.2 pixels. (*D*) EBCCD camera at 50 nm on the sample/pixel after the spatial correction. This is our standard condition used for simultaneous, dual-color, observations of single molecules. The standard deviations in terms of the pixels remained the same, but in the actual measurement, they were improved (scaled in proportion to the magnification) to 13 and 10 nm for the *x*- (*shaded*) and *y*- (*open*) directions, respectively.

x- and *y*-directions, respectively, with EBCCD cameras (Fig. 4 *C*, *left*; each pixel corresponding to 100 nm on the sample plane). CCD cameras are often used for scientific measurements, and when they are used, the spatial distortion by the camera is often neglected. However, these results indicated the possibility that the measurements could include an error of over a half-pixel (standard deviation) and possibly over a pixel in a particular region of the camera (see the distribution in Fig. 4 *C*, *left*), if the distortions were not corrected. After spatial correction, the accuracies were improved to 25 and 20 nm for 100 nm/pixel (0.25 and 0.2 pixels; Fig. 4 *C*, *right*) or 13 and 10 nm for 50 nm/pixel (0.26

and 0.2 pixels; Fig. 4 *D*) in the *x*- and *y*-directions, respectively. Because our normal two-color colocalization experiments of single molecules are carried out with the pixel size of ~50 nm, a superposition accuracy of 13 nm is probably generally achieved. These results indicate that the image superposition protocol developed here works well even for cameras with large distortions, like SIT tube cameras, and after the correction, the same levels of superposition accuracies can be achieved by the method described here.

Precision in position determination of single fluorescent molecules

The precision in the position determination of single fluorescent molecules in each image was evaluated under the conditions of simultaneous observations of two different fluorophores. For this purpose, Alexa633 conjugated to anti-CD59 Fab fragments (Alexa-Fab) and the recombinant GFP, produced in *E. coli* and purified, were attached to coverslips, which were and then covered with 15% polyacrylamide gel (thus immobilizing the molecules).

Typical images of these immobilized molecules (no averaging taken here) are shown in Fig. 5 *A*. The fluorescent spots are numbered in the order of integrated fluorescence intensity in each image, which will be related to the histograms in Fig. 5 *C*. Fig. 5 *B* shows typical single-molecule Alexa633 and GFP fluorescence intensities and the background intensities adjacent to the single-molecule spots, plotted as a function of time (video frames), showing the time-dependent fluctuations of the single-molecule fluorescence and the background signals. In Fig. 5 *C*, the distributions of the fluorescence intensities of the individual spots after background subtraction for each spot and the distributions of their background intensities (after subtracting the mean value) are shown for Alexa633 and GFP, respectively. (The fluorescence intensities of all of the observed spots in four independent images, like those shown in Fig. 5 *A*, were measured and plotted. In Fig. 5 *A*, only one quadrant of an image is shown.) The signal/noise (S/N) ratio for the single molecule fluorescent spot is given as

$$(I_S - I_B)/\sqrt{\sigma_S^2 + \sigma_B^2}, \quad (1)$$

where I_S is the signal intensity, I_B is the background signal intensity, and σ_S and σ_B are their respective standard deviations (Cheezum et al., 2001). Based on Eq. 1, we found signal/noise ratios of 2.7 and 2.6 for Alexa633 and GFP, respectively, in our instrument set up for simultaneous observations of Alexa633 and GFP (Table 1). Because Eq. 1 is true only when the noise components for the signal and the background are independent, and because, some noise, like that due to fluctuations of the laser power and the camera gain, may actually be spatially and temporally correlated, the true S/N ratio may be slightly better.

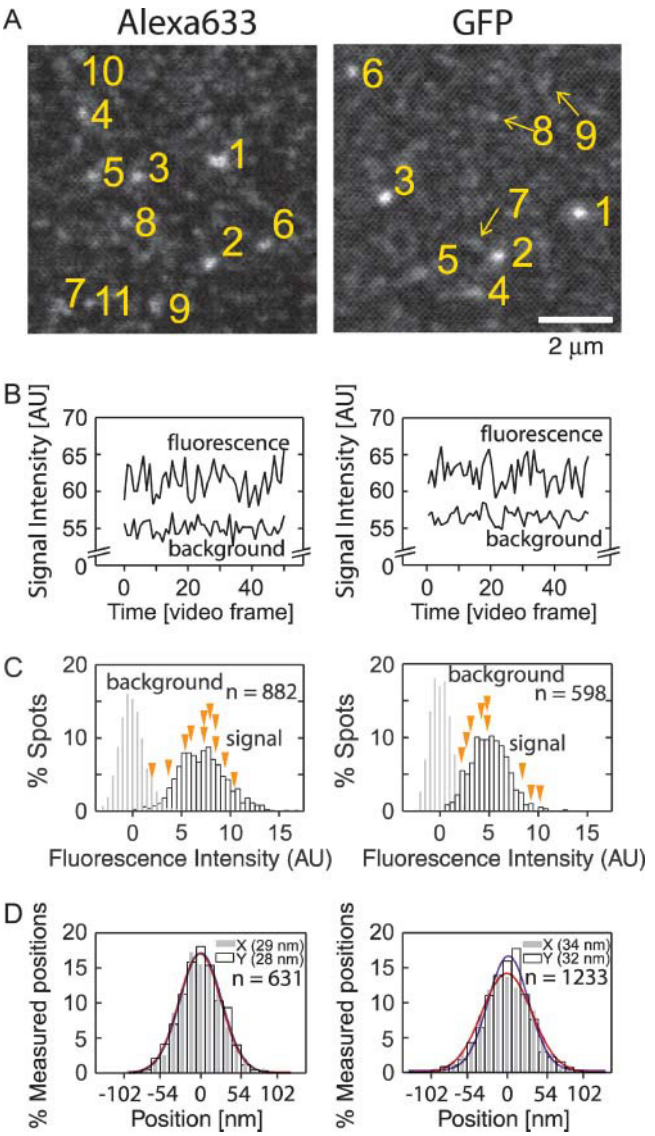

FIGURE 5 Simultaneous, dual-color, single-molecule observations of Alexa633 conjugated to anti-CD59 Fab fragments (Alexa633-Fab; *left column*; bottom port) and GFP (*right column*; side port) immobilized on the coverslips, to assess the signal/noise and signal/background ratios and the precision in determining the positions of these molecules. (*A*) Raw images of Alexa633-Fab and GFP adsorbed on coverslips. Scale bar = 2 μm. Single fluorescence spots are numbered in descending order of the signal intensity. (*B*) Typical fluorescence intensities of single molecules of Alexa633 and GFP, and the background intensities adjacent to the single-molecule spots, plotted as a function of time (video frames). (*C*) The distribution of the fluorescence signal intensity (after background subtraction for individual spots) and the background signal intensity (after subtraction of the mean value of the background signal). Yellow arrowheads indicate the intensities of the numbered fluorescence spots in panel *A*. (*D*) Histograms for the precisions in determining the coordinates of single fluorophores under the conditions of simultaneous, dual-color, single-fluorescent-molecule video observations (*x*, *shaded bars*; *y*, *open bars*). For ease of comparison, the mean value was subtracted from each determined value. The standard deviations of the distributions were 29 and 28 nm for Alexa633 (n = 631 determinations, 14 fluorophores) and 34 and 32 nm for GFP (n = 1233 determinations, 32 fluorophores) in the *x*- (Gaussian fit in *red line*) and *y*- (Gaussian fit in *blue line*) directions, respectively.

TABLE 1 Evaluation of the signal/noise ratios and the position determination precisions for single molecules of Alexa633 and GFP under simultaneous observation conditions

					Precision (nm)	
	I_S	I_B	$I_S - I_B$	S/N	x	y
Alexa633	64 ± 2.3	57 ± 1.3	7.2 ± 2.4	2.7	29	28
GFP	59 ± 1.6	54 ± 0.94	5 ± 1.9	2.6	34	32

Histograms of the measured positions for these fluorophores at this signal/noise ratio are shown in Fig. 5 *D*. For ease of comparison, the mean value for each coordinate was subtracted from all of the determined values. The widths (standard deviations) of these distributions are 29 (x) and 28 (y) nm for Alexa633 and 34 (x) and 32 (y) nm for GFP (Olympus 100× PlanApo, NA1.40; 2× tube lens; 2× projection lens; total magnification = 400×; 50 nm sample/pixel). Under the optimal conditions of observing single fluorescent molecules (by a single-color setup, and not a two-color setup), the standard deviations for localizing GFP are 32 and 33 nm in the x- and y-directions, respectively. Thus, even under the conditions of simultaneous observations of Alexa633-Fab and GFP, the localization precision was not reduced significantly.

Definition of colocalization for two chromatically separated images of single molecules of two different species

In this section, we develop a working definition of colocalization for the visualization of single GFP and Alexa633 molecules. We consider the accuracy of locating each fluorophore in their respective images (Alexa633, 29 and 28 nm; GFP, 34 and 32 nm; for 50 nm/pixel images by EBCCD cameras) and the accuracy of overlaying these images (13 and 10 nm for 50 nm/pixel images by EBCCD cameras) (in the horizontal and vertical directions, respectively). We combine these three distributions to determine the overall standard deviations, σ, between the two fluorophores in the overlapped images, obtaining $\sigma_x = \sqrt{29^2+34^2+13^2} = 47$ nm in the horizontal direction and $\sigma_y = \sqrt{28^2+32^2+10^2} = 44$ nm in the vertical direction.

These results indicate that even after the spatial correction between the side and bottom ports, the Alexa633 and GFP colocalized at the molecular level may appear to be 47 and 44 nm (one standard deviation, 68% of the total distribution) apart for the x- and y-directions, respectively. For simplicity, we will use 45 nm as the standard deviation of the ''displacement'' for each direction and 64 nm as that of the ''distance'' between the two spots. Note that if fluorophores with higher signal levels, such as fluorescent beads and semiconductor nanocrystal quantum dots, could be employed, the colocalization accuracy would improve greatly.

To ascertain 90% probability that two colocalized molecules are in fact judged as colocalized, the definition of colocalization has to be loosened so that two molecules may be designated as being colocalized when they are within 1.65σ, i.e., within 74 nm in displacements in both the horizontal and vertical directions, or within 100 nm in distance after overlaying the spatially corrected images. As the definition becomes less strict, the chances of missing true colocalization decrease, but the chances of erroneously including a pair of molecules incidentally passing by each other increase. However, the latter possibility could be reduced, for example, by reducing the number of probe molecules in the image or by examining consecutive image frames. Although the value of 100 nm is 10–50-fold greater than the size of a protein, and this by itself may be insufficient for colocalization at the molecular level, for molecules in motion, colocalization could be defined much more precisely by including a time-dependent definition of colocalization. Because molecules can diffuse in the membrane with diffusion coefficients of 0.3–3 $\mu m^2/s$ (when viewed at 30 Hz) (Chang et al., 1981; Fujiwara et al., 2002; Kusumi et al., 1993; Murase et al., 2004; Sako and Kusumi, 1994; Tomishige et al., 1998; Vrljic et al., 2002), during one frame at the standard video rate, the molecules in the plasma membrane can cover an area with a radius of 200–700 nm. Therefore, if two molecules are located within 100 nm over several video frames after the corrections for spatial distortions proposed here, it is likely that an interaction or binding of these two molecules is occurring. Such a definition depends on the motion of individual molecular species, and has to be considered for each case.

Determination of the actual precision of colocalization of simultaneous, dual-color, fluorescence images of single molecules

The precision for colocalization of two single fluorescent molecules was estimated by attaching anti-E-cadherin Fab conjugated with Alexa633 (Alexa-αEcad-Fab) to E-cadherin-GFP (Ecad-GFP) expressed on the surface of L cells (fixed), and then by examining the distribution of the displacement between single molecules of Ecad-GFP and Alexa-Ecad-Fab (Fig. 6). Because E-cadherin molecules on the cell surface exhibit various levels of clustering (Iino et al., 2001), only the fluorescent spots with fluorescence intensities within the single molecule range in the histograms shown in Fig. 5 *C* were selected. All of these fluorescent spots were identified in eight independent images for each color, and between the synchronously obtained images, the distances of all of the possible pairs of GFP and Alexa633 were measured. We found 163 pairs of E-cad-GFP and Alexa-αEcad-Fab with *distances* within 100 nm of each other, and selected them as candidates for bound pairs. The distributions of the *displacements* between these candidate

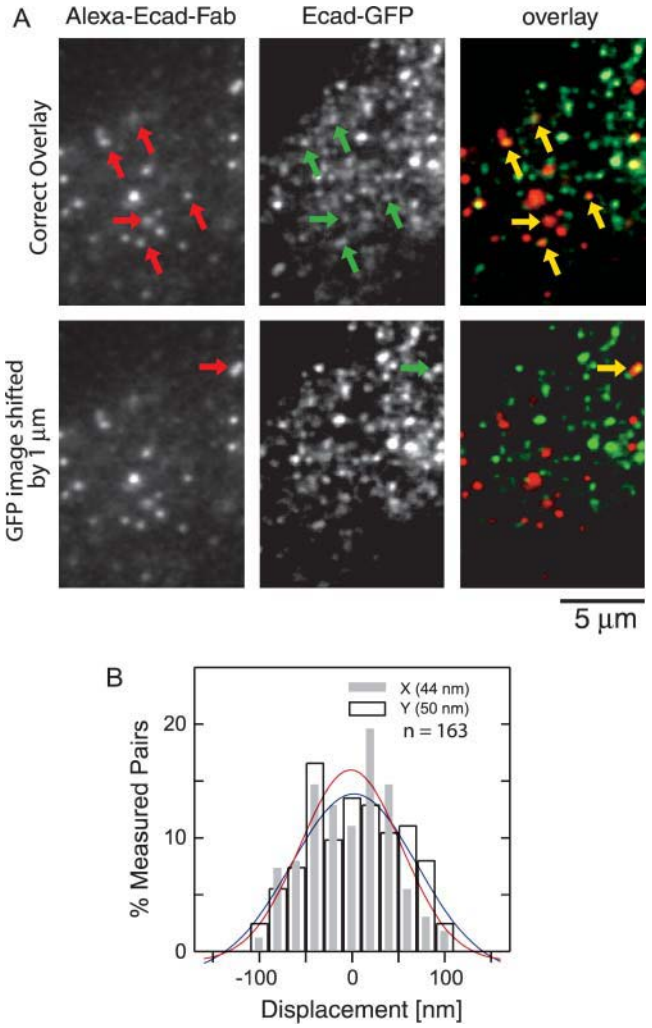

FIGURE 6 Simultaneous, dual-color, fluorescence observations of single molecules of Alexa-αEcad-Fab (*red*, bottom port) bound to Ecad-GFP (*green*, side port) on a fixed L cell. (*A*, *top*) Representative synchronously obtained, spatially corrected images of Alexa-αEcad-Fab (*left*) and Ecad-GFP (*middle*), and their overlaid images (*right*). For this display, only a small part of a typical 640- $\times$ 480-pixel image is shown (and, therefore, the number of colocalized spots is small in these figures). Arrows show colocalized spots (within 100 nm of each other). Only the spots with single-molecule fluorescence intensities were selected. (*A*, *bottom*) As a control, the corrected E-cad-GFP image was shifted toward left by 1 μm and overlaid with the corrected image of Alexa-αEcad-Fab. Only one incidental overlap (shown by a *yellow arrow*) was found here. The scale bar indicates 5 μm. (*B*) The distributions of the *x*- and *y*-displacements for pairs found to be separated within 100 nm (note that this is the true distance between the two spots, rather than the displacements in the *x*- and *y*-directions). All of the spots with single-molecule signal intensities were identified in each color (eight independent images for each color). The distances of all pairs of green and red spots in the synchronous images were measured, and those within 100 nm were selected (163 pairs). The standard deviations of the displacements for these pairs were 44 and 50 nm in the horizontal (Gaussian fit in *red line*) and vertical (Gaussian fit in *blue line*) directions, respectively.

pairs are shown in the histograms shown in Fig. 6 *B*. The standard deviations of the displacements between these fluorophores were 44 and 50 nm in the *x*- and *y*-directions, respectively, indicating that the standard deviation of the distance between the pair was 67 nm, consistent with the prediction of 64 nm.

As a control for the incidental overlap, we apply an empirical method to determine the number of coincidental colocalizations in each experiment. This procedure is shown in Fig. 6 *A* (*bottom*) using the same Alexa-αEcad-Fab/Ecad-GFP image as an example: the number of coincidental colocalizations is estimated by shifting one image (Ecad-GFP) by 1 μm with respect to the image from the other observation arm (Alexa-αEcad-Fab). As compared with top images of Fig. 6 *A*, which are correctly overlaid, we could find only one pair of Ecad-GFP and Alexa-αEcad-Fab molecules with distance within 100 nm. We investigated the six images of 240 $\times$ 260 pixel area where we found a total of five pairs of E-cad-GFP and Alexa-αEcad-Fab in the shifted, overlaid images, which can be compared to the 43 pairs found in the same images that were correctly overlaid. Therefore, we could estimate that the error of detection of colocalization under the threshold of 100 nm is $\sim$12% in this particular case. The error levels vary depending on the density and distribution of the fluorescent spots, and therefore the coincidental overlaps always have to be examined for all of the paired images captured simultaneously.

Note that the superposition accuracy of 64 or 100 nm is a factor of 3–6 smaller than the Rayleigh limit for resolving two points in a single image. This is not surprising, because the precision with which the single spots can be localized is much greater than the resolving limitation (Anderson et al., 1992; Gelles et al., 1988).

Demonstration of simultaneous, dual-color, fluorescence imaging of single molecules for the colocalization detection of membrane molecules diffusing in the plasma membrane of living cells

To demonstrate this technique in *live* cells for observing colocalization of two single molecules, we observed Ecad-GFP labeled on its extracellular domain with Alexa-αEcad-Fab, diffusing in the plasma membrane in live L cells. Simultaneous, dual-color, fluorescence video imaging of GFP and Alexa at the single-molecule level was carried out at 37°C (30 Hz, i.e., every 33 ms), and a series of synchronized raw images of Ecad-GFP and Alexa-αEcad-Fab (210 frames each for 7 s) were spatially corrected and superimposed by the method described in Fig. 3 (Fig. 7; also see Supplementary Material). As described previously (Iino et al., 2001), Ecad forms oligomers on the cell surface, and therefore, the fluorescent spots within single-molecule fluorescence intensities were selected and used for the examinations here.

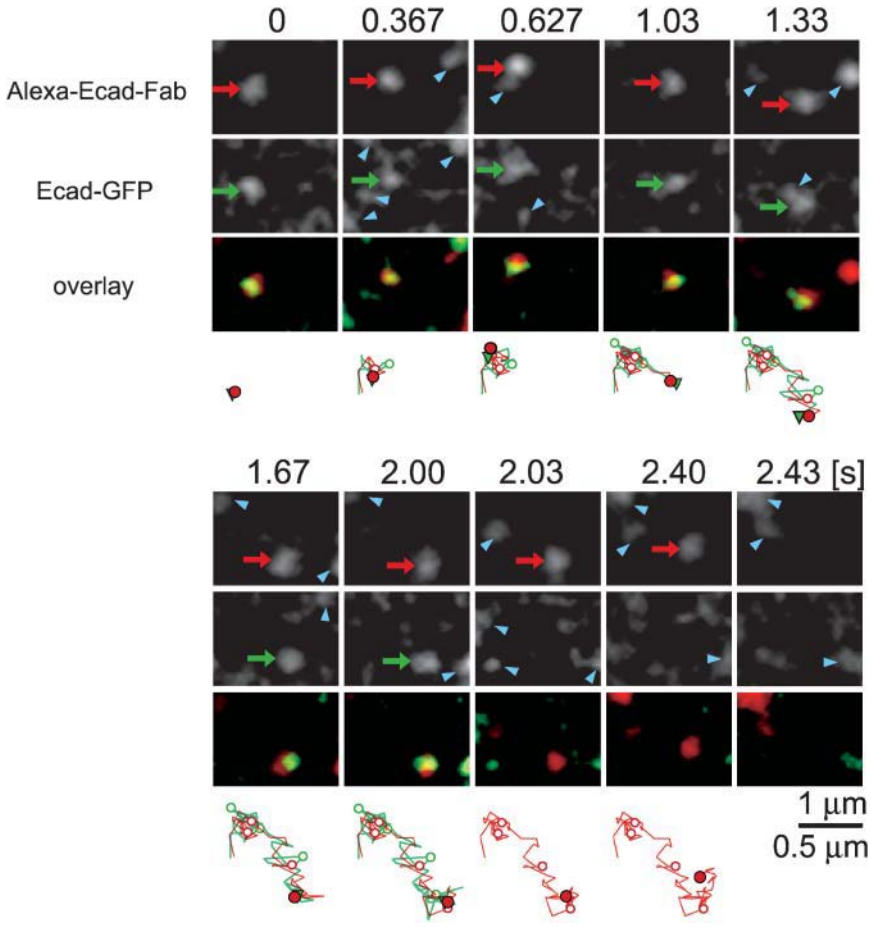

FIGURE 7 Detection of colocalization of single molecules diffusing in the plasma membrane of living cells. Ecad-GFP (green) and Alexa-αEcad-Fab (red) on the living L-cell surface were simultaneously imaged using dual-color, single-molecule, fluorescence video imaging (observed at the normal video rate of 30 Hz). Spatially corrected, superimposed video images (see Supplementary Material) are shown. A green fluorescent spot, representing an Ecad-GFP molecule (indicated by *green arrows*), was colocalized with a red Alexa-αEcad-Fab spot (indicated by *red arrows*). Other spots representing single molecules are shown by blue arrowheads. The fluorescence intensities appear to vary greatly from spot to spot, but they rather represent time-dependent changes of the intensity, due to the spatiotemporal fluctuations of the signal intensification level of the image intensifier. The selected colocalized spots (indicated by *green* and *red arrows*) are those that exhibited relatively small variations in intensity during the observation period. Beneath each image, the concurrent positions (*green triangles* and *red circles*) and the trajectories of these spots are shown (note the different scales; the bar indicates 1 μm for the images and 0.5 μm for the trajectories). An Ecad-GFP molecule and an Alexa-αEcad-Fab molecule diffused together on the cell membrane for 2 s, keeping their distances basically within 100 nm. The open circles in the trajectories indicate the coordinates where the red and green spots lost colocalization, but which is limited for a single frame (see text). There are four circles in each trajectory (which is 61 frames long). The Ecad-GFP molecule showed a one-step photobleaching in one video frame (2.00–2.03 s), but the Alexa-αEcad-Fab molecule was still observable and kept diffusing for another 0.4 s until finally it was photobleached (or released from the cell surface) over a single video frame (2.40–2.43 s). At 2.03 and 2.40 s, the green trajectories are not shown to indicate that the green spot was photobleached, and likewise, the red trajectory is not shown at the last time point (2.43 s)

In Fig. 7, at time 0, a single molecule of Alexa-αEcad-Fab and a single molecule of Ecad-GFP were colocalized. Both of these spots diffused in a similar way, as shown in trajectories shown in Fig. 7, keeping their colocalization to each other (they were basically within 100 nm to each other, but see below). The problem of using live cell samples for single fluorescent molecule imaging is that the fluorescence intensities of single spots fluctuate much more greatly in live cells than in fixed cells. Therefore, a fluorescent spot representing a single molecule may occasionally become too dim for the calculation of its location or the distances between two fluorescent spots may become >100 nm. But, these tend to last only for a single observation frame. In this example, if these lasted only for a single frame, and if the signal intensity came back to the normal level or the colocalization of the two spots was recovered in the next fame, then they were counted as a part of the colocalization period. The spot that disappeared for a single frame was assumed to be present at the middle point between the two adjacent spots in the trajectory. To show the transient loss of colocalization for just a single frame in the trajectories shown in Fig. 7, the locations of the pair in such instances are displayed with open circles.

This particular pair shown in Fig. 7 exhibited colocalization until 2.00 s. In the next frame, the Ecad-GFP spot was gone, suggesting a single-step photobleaching, confirming that this Ecad-GFP represented a single molecule of Ecad-GFP. The Alexa spot disappeared in a single frame from 2.40 to 2.43 s, again confirming that this spot originated from a single Alexa-αEcad-Fab molecule. The diffusion coefficients in the time window of 67 ~ 267 ms averaged over this whole colocalization period were 0.047 and 0.037 $\mu m^2/s$ for Ecad-GFP and Alexa-αEcad-Fab, respectively, showing a reasonable agreement. These results indicate that the fluorescence single-molecules colocalization method developed here works well for membrane molecules in living cells.

CONCLUSIONS

Many cellular processes require the concerted action of two or more molecules, each entering and exiting the site of action in a specific and dynamic way. We have described

a simple, practical method to observe and detect the colocalization of two molecules accurately at the single molecule level, by performing a rapid spatial correction for an entire sequence of full-frame images. The spatial correction only involves the imaging of arrays of optically transparent holes, using white-light transmission bright-field microscopy with detection at the two different wavelengths used for the fluorescence experiment, and then the spline-fit correction of the two images to the original array. By using our full-frame image correction technique, two molecules can be localized to within 64 nm (68% detectability) or 100 nm (90% detectability) in the plasma membrane of living cells. The spatial correction enables the superposition of green (GFP wavelength) and red (Alexa633 wavelength) images with 13-nm accuracy. Thus, after this spatial correction, the major limitation for the superposition accuracy of two single fluorescent molecules (with these two colors) was found to be the precision of determining the position of the individual fluorescent spot, rather than the problems with the microscope optics and the camera. Therefore, improvements of poor signal/noise and signal/background ratios in single-molecule imaging will be an important next step in this field. The same method can be applied to two-color images obtained by a single camera (Kinosita et al., 1991; however, for the practical purpose of performing complex single-molecule two-color simultaneous observations, it is much easier to have two separate gain controls over each of two cameras, rather than trying to use a single camera with the spatial or temporal shifts of images with two different colors).

Our procedure for image correction, when applied to molecules diffusing in the membrane, will allow the extension of the definition of colocalization to include the probability that the two molecules, while diffusing in the membrane, stay within 100 nm of each other. This is a much more robust measure of colocalization, and work for including diffusion in colocalization detection is in progress in our laboratory.

As another approach for a higher degree of precision in determining molecular colocalization, one may be able to employ single-molecule FRET between the two molecules of interest (Murakoshi et al., 2004; Schütz et al., 1998). In this case, the image correction and overlay technique described here allows for the accurate determination of single-molecule FRET as well as the precise overlay of the fluorescent images, before, during, and after the occurrence of FRET. This allows the dynamics of the interaction to be fully explored (Murakoshi et al., 2004).

When the method developed here was applied to the observation of a doubly labeled E-cadherin molecule in the plasma membrane of a live cell, the signals from the two fluorophores were found to colocalize over several seconds even in the presence of the diffusion of the E-cadherin molecule. In fact, the register of the two molecules in the presence of diffusion further strengthens the definition of colocalization due to the fact that two independent diffusing molecules at $\sim$0.04 $\mu m^2/s$ will not stay within our defined 100 nm for such a long period of time (2 s). Therefore, this method will provide a powerful tool for studying interactions of signaling molecules at the level of single molecules in live cells, where the dynamics of the process can be functionally important. Such approaches will allow the critical testing of many current hypotheses in cell biology, as the interaction, binding, and colocalization of molecules are fundamental issues to be elucidated in the studies of a variety of cellular processes.

APPENDIX: DETAILS OF THE SPATIAL CORRECTION OF THE IMAGES

To transform the raw video image into the spatially corrected image, we perform the following procedure. The image of the mask forms an array of $M \times N$ points on the image. The corrected image should have these points in a square array separated by 5 μm between the points. We choose a final spatial resolution that is close to the spatial resolution of the raw image at its center usually $\sim$50 nm/pixel. The positions of the points in the array on the raw image are (X^{mn}, Y^{mn}), where the upper indices refer to the position in the array at column $m = 0 \ldots M-1$ and row $n = 0 \ldots N-1$. These points are parameterized with respect to the horizontal pixel position of the corresponding point in the array in the corrected image, that is $(X^{mn}(m \times p), Y^{mn}(m \times p))$, where p is the number of pixels between each point of the array in the corrected image ($p = 100$ for 50 nm/pixel and 5 μm between points). For each row n, cubic spline interpolation is employed for both sets of $X^{mn}(m \times p)$ and $Y^{mn}(m \times p)$, separately. From this, we can interpolate the position in the raw image, $\left({}^{x}S_i^n, {}^{y}S_i^n\right)$ on row n, that corresponds to the pixel in row n at pixel position $i = 0 \ldots (M-1)p$ in the corrected image. The interpolation is done such that between two adjacent points of the array on any row, there are p equally spaced points (pixels). At this point, we have a corresponding location on the raw image for all of the pixels that reside between the points of the mask array on any row. To fill in the rest of the points, cubic spline interpolation is once again employed. Along the corresponding interpolated points in each row at a horizontal pixel position, $\left({}^{x}S_i^0(0), {}^{x}S_i^1(p), \ldots, {}^{x}S_i^{N-1}((N-1)p)\right)$ and $\left({}^{y}S_i^0(0), {}^{y}S_i^1(p), \ldots, {}^{y}S_i^{N-1}((N-1)p)\right)$, parameterized with respect to their vertical pixel location in the destination corrected image, a spline interpolation is performed to estimate the location on the raw image $\left({}^{x}T_{ij}, {}^{y}T_{ij}\right)$ corresponding to the pixel $(i, j), i = 1 \ldots (M-1)p, j = 1 \ldots (N-1)p$ on the destination corrected image. Thus, a mapping between the intensity found at location $\left({}^{x}T_{ij}, {}^{y}T_{ij}\right)$ (determined by the nearest neighbor method) on the raw image and the intensity to be written to location (i, j) in the corrected image is determined, and can be applied to all subsequent frames of the video.

SUPPLEMENTARY MATERIAL

An online supplement to this article can be found by visiting BJ Online at http://www.biophysj.org.

We thank Ms. Junko Kondo of our laboratory for her help in making figures, and the members of the Kusumi lab for helpful discussion.

REFERENCES

Anderson, C. M., G. N. Georgiou, I. E. Morrison, G. V. Stevenson, and R. J. Cherry. 1992. Tracking of cell surface receptors by fluorescence digital imaging microscopy using a charge-coupled device camera.

Low-density lipoprotein and influenza virus receptor mobility at 4 degrees C. *J. Cell Sci.* 101:415–425.

Chang, C. H., H. Takeuchi, T. Ito, K. Machida, and S. Ohnishi. 1981. Lateral mobility of erythrocyte membrane proteins studied by the fluorescence photobleaching recovery technique. *J. Biochem. (Tokyo).* 90:997–1004.

Cheezum, M. K., W. F. Walker, and W. H. Guilford. 2001. Quantitative comparison of algorithms for tracking single fluorescent particles. *Biophys. J.* 81:2378–2388.

Derrick, J. P., and D. B. Wigley. 1994. The third IgG-binding domain from streptococcal protein G. An analysis by X-ray crystallography of the structure alone and in a complex with Fab. *J. Mol. Biol.* 243:906–918.

Fujiwara, T., K. Ritchie, H. Murakoshi, K. Jacobson, and A. Kusumi. 2002. Phospholipids undergo hop diffusion in compartmentalized cell membrane. *J. Cell Biol.* 157:1071–1081.

Gelles, J., B. J. Schnapp, and M. P. Sheetz. 1988. Tracking kinesin-driven movements with nanometre-scale precision. *Nature.* 331:450–453.

Iino, R., I. Koyama, and A. Kusumi. 2001. Single molecule imaging of green fluorescent proteins in living cells: E-cadherin forms oligomers on the free cell surface. *Biophys. J.* 80:2667–2677.

Karakikes, I., R. E. Barber, I. E. Morrison, N. Fernandez, and R. J. Cherry. 2003. Co-localization of cell surface receptors at high spatial resolution by single-particle fluorescence imaging. *Biochem. Soc. Trans.* 31:1453–1455.

Kinosita, K., Jr., H. Itoh, S. Ishiwata, K. Hirano, T. Nishizaka, and T. Hayakawa. 1991. Dual-view microscopy with a single camera: real-time imaging of molecular orientations and calcium. *J. Cell Biol.* 115:67–73.

Kusumi, A., Y. Sako, and M. Yamamoto. 1993. Confined lateral diffusion of membrane receptors as studied by single particle tracking (nanovid microscopy). Effects of calcium-induced differentiation in cultured epithelial cells. *Biophys. J.* 65:2021–2040.

Lacoste, T. D., X. Michalet, F. Pinaud, D. S. Chemla, A. P. Alivisatos, and S. Weiss. 2000. Ultrahigh-resolution multicolor colocalization of single fluorescent probes. *Proc. Natl. Acad. Sci. USA.* 97:9461–9466.

Lommerse, P. H., G. A. Blab, L. Cognet, G. S. Harms, B. E. Snaar-Jagalska, H. P. Spaink, and T. Schmidt. 2004. Single-molecule imaging of the H-ras membrane-anchor reveals domains in the cytoplasmic leaflet of the cell membrane. *Biophys. J.* 86:609–616.

Mashanov, G. I., D. Tacon, M. Peckham, and J. E. Molloy. 2004. The spatial and temporal dynamics of pleckstrin homology domain binding at the plasma membrane measured by imaging single molecules in live mouse myoblasts. *J. Biol. Chem.* 279:15274–15280.

Morrison, I. E., I. Karakikes, R. E. Barber, N. Fernandez, and R. J. Cherry. 2003. Detecting and quantifying colocalization of cell surface molecules by single particle fluorescence imaging. *Biophys. J.* 85:4110–4121.

Murakoshi, H., R. Iino, T. Kobayashi, T. Fujiwara, C. Ohshima, A. Yoshimura, and A. Kusumi. 2004. Single-molecule imaging analysis of Ras activation in living cells. *Proc. Natl. Acad. Sci. USA.* 101:7317–7322.

Murase, K., T. Fujiwara, Y. Umemura, K. Suzuki, R. Iino, H. Yamashita, M. Saito, H. Murakoshi, K. Ritchie, and A. Kusumi. 2004. Ultrafine membrane compartments for molecular diffusion as revealed by single molecule techniques. *Biophys. J.* 86:4075–4093.

Perosa, F., G. Luccarelli, M. Neri, and F. Dammacco. 1997. The Fab region of IgG2 human myeloma proteins does not bear the streptococcal protein G-specific determinant. *J. Immunol. Methods.* 203:153–155.

Sako, Y., and A. Kusumi. 1994. Compartmentalized structure of the plasma membrane for receptor movements as revealed by a nanometer-level motion analysis. *J. Cell Biol.* 125:1251–1264.

Sako, Y., S. Minoghchi, and T. Yanagida. 2000. Single-molecule imaging of EGFR signalling on the surface of living cells. *Nat. Cell Biol.* 2:168–172.

Sako, Y., A. Nagafuchi, S. Tsukita, M. Takeichi, and A. Kusumi. 1998. Cytoplasmic regulation of the movement of E-cadherin on the free cell surface as studied by optical tweezers and single particle tracking: corralling and tethering by the membrane skeleton. *J. Cell Biol.* 140:1227–1240.

Schütz, G. J., G. Kada, V. P. Pastushenko, and H. Schindler. 2000. Properties of lipid microdomains in a muscle cell membrane visualized by single molecule microscopy. *EMBO J.* 19:892–901.

Schütz, G. J., W. Trabesinger, and T. Schmidt. 1998. Direct observation of ligand colocalization on individual receptor molecules. *Biophys. J.* 74:2223–2226.

Sheetz, M. P., S. Turney, H. Qian, and E. L. Elson. 1989. Nanometre-level analysis demonstrates that lipid flow does not drive membrane glycoprotein movements. *Nature.* 340:284–288.

Shirayoshi, Y., A. Nose, K. Iwasaki, and M. Takeichi. 1986. N-linked oligosaccharides are not involved in the function of a cell-cell binding glycoprotein E-cadherin. *Cell Struct. Funct.* 11:245–252.

Suzuki, K., T. Fujiwara, K. Ritchie, F. Sanematsu, H. Hirano, M. Edidin, and A. Kusumi. 2004. Rapid diffusion of putative raft molecules indicative of the absence of large stable rafts in the resting-state cell membrane. *Biophys. J.* 86:9 (Abstr.).

Suzuki, K., F. Sanematsu, T. Fujiwara, K. Ritchie, M. Edidin, and A. Kusumi. 2003. Crosslinking of a GPI-anchored protein creates signaling rafts from smaller, transient, lipid rafts. *Biophys. J.* 84:487 (Abstr.).

Tardin, C., L. Cognet, C. Bats, B. Lounis, and D. Choquet. 2003. Direct imaging of lateral movements of AMPA receptors inside synapses. *EMBO J.* 22:4656–4665.

Tomishige, M., Y. Sako, and A. Kusumi. 1998. Regulation mechanism of the lateral diffusion of band 3 in erythrocyte membranes by the membrane skeleton. *J. Cell Biol.* 142:989–1000.

Trabesinger, W., B. Hecht, U. P. Wild, G. J. Schutz, H. Schindler, and T. Schmidt. 2001. Statistical analysis of single-molecule colocalization assays. *Anal. Chem.* 73:1100–1105.

Vrljic, M., S. Y. Nishimura, S. Brasselet, W. E. Moerner, and H. M. McConnell. 2002. Translational diffusion of individual class II MHC membrane proteins in cells. *Biophys. J.* 83:2681–2692.